Computer simulation of structures and rheological properties of electrorheological fluids

H. X. Guo,[1] Z. H. Mai,[1] and H. H. Tian[2]
[1]*Institute of Physics, Chinese Academy of Sciences, P.O. Box 603, Beijing 100080, People's Republic of China*
[2]*P.O. Box 2851, Beijing 100085, People's Republic of China*
(Received 2 June 1995; revised manuscript received 27 October 1995)

The structural phase diagram of electrorheological (ER) fluids as a function of dimensionless parameters λ (the ratio of the dipolar force to the Brownian force) and Pe (the ratio of the shear force to the Brownian force) is constructed. In the phase diagram, there exist three single phases: a layerlike or chainlike crystalline phase (C), a shear-string phase (S), and a liquid phase (L). Between these single phases two phase coexistence zones of $C+S$ and $C+L$ are located. The transitions between the phases are driven by the competition between the dipolar, shear, and Brownian forces. In the different phase zones, the viscosity of the ER fluid has different dependencies on Pe and λ. The observed structures and corresponding rheological properties are discussed.

PACS number(s): 83.80.Gv, 83.20.Jp, 83.20.Hn, 83.50.Ax

I. INTRODUCTION

In view of their great potential in industrial application, electrorheological (ER) fluids have stimulated considerable interest in recent years [1]. A typical ER fluid is a colloidal suspension of fine dielectric particles in a low conductive liquid [2–4]. In the presence of a large electric field, chainlike or columnlike structures are formed parallel to the field, and dramatical changes of the rheological properties of the suspension such as stress and viscosity occur in a few milliseconds.

The structure is a key to understanding the physical mechanism of this phenomenon. At present a few three-dimensional (3D) simulations of ER fluids in the static state (without shear flow) have been reported. Although Hass found that a regular lattice was not formed in his 3D simulation [5], a simulation by Tao revealed that a body-centered-tetragonal (bct) structure formed as a result of the Brownian and dipolar forces [6]. In fact, most ER fluids are employed in the dynamic state (under shear flow). For these cases, simulations should accurately account for the hydrodynamic interaction. Methods for the complete treatment of hydrodynamic force have been developed. However, the treatment is computationally expensive, limiting studies to a small 2D system of 25 particles [7]. To understand structures in the sheared suspension, it is necessary to retain three dimensions. Equally important, to obtain accurate statistics it is necessary to simulate a large number of particles with extensive averaging. We have therefore abandoned such complicated hydrodynamic effects and adopted, like other authors [8–11], an idealized $O(N^2)$ algorithm: free draining particle suspensions with uncorrelated Brownian motion subjected to a homogeneous shear flow. Because of the simplicity of this algorithm, we can simulate many particles in 3D and preserve the essential symmetries of the particle interactions and the shear flow. Melrose [11] investigated the nonequilibrium phase diagram of ER fluids by applying an increasing electric field to a suspension already sheared at a fixed shear rate. Four distinct phases existed: the layered phase, shear-string phase, and two kinds of liquid phases. However, the curvature in the boundaries between the phases and the meeting of the phases were not resolved. In the present work, we adopt another trajectory to explore the 3D structures and rheological properties of ER fluids: that is, by applying a shear with different shear rate into a suspension which is already exposed to a fixed electric field. This procedure is equivalent to the experimental situation of applying an electric field to a suspension at zero shear rate for a certain time prior to applying the shear.

II. MODEL

An ER fluid is modeled here as a neutrally buoyant suspension of spherical particles with diameter σ and dielectric constant ε_p in a nonconductive solvent of dielectric constant ε_f and viscosity η. The fluid is confined between two parallel-plate electrodes with a separation L_z. The homogeneous shear flow is placed on the ER fluid by sliding the top electrode. The full computational geometry is summarized in Fig. 1, where z is chosen as the direction of an applied electric field $E_0\mathbf{e}_z$, x the direction of an imposed shear flow at a rate $\dot{\gamma}\mathbf{e}_x$, and y the direction of the vortical axis. The two unit vectors $\mathbf{e}_r$ and $\mathbf{e}_\theta$ are parallel to and perpendicular to the line joining the two particles, respectively, and θ_{ij} is the angle between $\mathbf{e}_z$ and $\mathbf{e}_r$. For simplification, we assume that the particles freely rotate in the shear flow, and remain polarized along the z direction. Before the application of an electric field, the particles are randomly distributed in the fluid. When the field is applied, each particle acquires an induced dipole moment $\mathbf{P}=\beta\varepsilon_f(\sigma/2)^3\mathbf{E}_{\rm loc}$, where $\beta=(\varepsilon_p-\varepsilon_f)/(\varepsilon_p+2\varepsilon_f)$ and $\mathbf{E}_{\rm loc}$ is the local field, $\mathbf{E}_{\rm loc}=E_0\mathbf{e}_z$ if $\beta\ll 1$. The motion of the ith particle is described by [10]

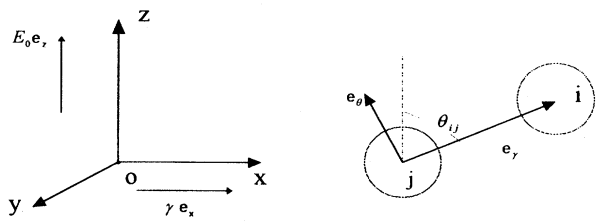

FIG. 1. The computational geometry.

$$m d^2\mathbf{r}_i/dt^2 = \mathbf{F}_i - 3\pi\sigma\eta(d\mathbf{r}_i/dt - \dot{\gamma} z_i \mathbf{e}_x) + \mathbf{R}_i , \quad (1)$$

where m is the mass of the ith particle and $\mathbf{r}_i$ its position at time t. $\mathbf{F}_i$ is the interparticle force on it, including both the long-range dipolar and short-range repulsive forces; $-3\pi\sigma\eta(d\mathbf{r}_i/dt - \dot{\gamma} z_i \mathbf{e}_x)$ is the Stokes drag force and $\mathbf{R}_i$ is the Brownian force, both acting on it through the solvent. The dipolar force on the ith particle due to a particle at $\mathbf{r}_j$ is

$$\mathbf{F}_{ij}^{d} = [3p^2/(\varepsilon_f r_{ij}^4)][(1-3\cos^2\theta_{ij})\mathbf{e}_r - \sin(2\theta_{ij})\mathbf{e}_\theta], \quad (2)$$

where $r_{ij} = [(x_i - x_j)^2 + (y_i - y_j)^2 + (z_i - z_j)^2]^{1/2}$. A particle can produce an infinite number of reflected images about the electrodes. The force between a particle and an image has the same form as Eq. (2). $\mathbf{F}_{ij}^{d'}$ is the summation force on particle i due to the images of particle j. To simulate the hard spheres and the hard sphere/hard wall interactions, we introduce an exponential short-range repulsive force between particles i and j,

$$\mathbf{F}_{ij}^{\mathrm{rep}} = [3p^2/(\varepsilon_f r_{ij}^4)]\exp[-100(r_{ij}/\sigma - 1)]\mathbf{e}_r , \quad (3)$$

and between particle i and the two electrodes

$$\mathbf{F}_i^{\mathrm{wall}} = ([3p^2/(\varepsilon_f z_i^4)] \times \exp[-100(z_i/\sigma - 0.5)] - \{3p^2/[\varepsilon_f (L_z - z_i)^4]\} \times \exp\{-100[(L_z - z_i)/\sigma - 0.5]\})\mathbf{e}_z . \quad (4)$$

Unlike Melrose's simulation [11], the repulsive force is dependent on the dipolar interaction. Now $\mathbf{F}_i$ in Eq. (1) is given by $\mathbf{F}_i = \Sigma_{j\neq i}(\mathbf{F}_{ij}^{d} + \mathbf{F}_{ij}^{\mathrm{rep}}) + \Sigma_j \mathbf{F}_{ij}^{d'} + \mathbf{F}_i^{\mathrm{wall}}$. The Brownian force $\mathbf{R}_i$ is determined independently by a normal distribution with $\langle R_{i,\alpha}\rangle = 0$ and $\langle R_{i,\alpha}(0) R_{i,\beta}(t)\rangle = 6\pi k_B T \sigma \eta \delta_{\alpha\beta}\delta(t)$, where k_B is Boltzmann's constant and T is the temperature. We scale Eq. (1) by defining dimensionless quantities: $\mathbf{r}_i^* = \mathbf{r}_i/\sigma$, $t^* = t/(3\pi\eta\sigma^3/k_B T)$, $\mathbf{R}_i^* = \mathbf{R}_i/(k_B T/\sigma)$, and $\mathbf{F}_i^* = \mathbf{F}_i/(p^2/\varepsilon_f\sigma^4)$, so Eq. (1) becomes

$$[mk_B T/(3\pi\eta\sigma^2)^2] d^2\mathbf{r}_i^*/dt^{*2} = \lambda \mathbf{F}_i^* - d\mathbf{r}_i^*/dt^* + 8\mathrm{Pe} z_i^* \mathbf{e}_x + \mathbf{R}_i^* , \quad (5)$$

where two dimensionless parameters $\lambda = p^2/(\varepsilon_f\sigma^3 k_B T)$ and $\mathrm{Pe} = 3\pi\eta\sigma^3\dot{\gamma}/(8k_B T)$. The λ characterizes the ratio of the dipolar force to the Brownian force, and Pe represents the dimensionless shear rate setting the ratio of the shear force to the Brownian force. For most real parameters, the magnitude in the square brackets of Eq. (5) is very small ($\sim 10^{-10}$), so the inertial effect can be neglected. Then Eq. (5) is simplified as

$$d\mathbf{r}_i^*/dt^* = \lambda \mathbf{F}_i^* + 8\mathrm{Pe} z_i^* \mathbf{e}_x + \mathbf{R}_i^* . \quad (6)$$

According to Eq. (6), in the dynamic state the behavior of the suspension is dependent on the competition between λ, Pe, and unit 1 (representing the dimensionless magnitude of the Brownian force), while in the static state it is determined by the magnitude of λ. Equation (6) is integrated with a time step $\Delta t^* \leq 0.001/\lambda$ using Euler's method. A system of $N = 200$ particles in a box with $L_z^*/3 = L_y^* = L_x^* = 5$ is simulated along many trajectories in the space (λ,Pe). At each state point, averages are taken over 10^4 time steps. The particle volume fraction is 0.28. To examine the structural changes of the suspension, the top electrode is translated over $5L_x$ (shear strain above $\frac{5}{3}$) until the suspension comes to the stable state. Periodic boundary conditions are imposed in the x and y directions, reflecting boundaries at the electrodes.

During simulation, equilibrium structures in the static state were probed by the following three order parameters:

$$\rho_j = \left| \frac{1}{N} \sum_{i=1}^{N} \exp(i\mathbf{b}_j \cdot \mathbf{r}_i) \right| \quad (j = 1,2,3), \quad (7)$$

where the three reciprocal lattice vectors of the bct lattice are $\mathbf{b}_1 = (2\pi/\sigma)(2\mathbf{e}_x/\sqrt{6} - \mathbf{e}_z)$, $\mathbf{b}_2 = (2\pi/\sigma)(2\mathbf{e}_y/\sqrt{6} - \mathbf{e}_z)$, and $\mathbf{b}_3 = 4\pi\mathbf{e}_z/\sigma$. In these order parameters, ρ_3 characterizes the formation of chains in the z direction, while ρ_1 and ρ_2 characterize the structure of particle arrangement in the x-y plane. In the dynamic state, because equilibrium structures can be pulled into a number of layers in which the particles have a hexagonal structure normal to the y direction, or shear strings which form a distorted hexagonal pattern in the y-z plane, the nonequilibrium structures were examined not only by the average $\langle p_j\rangle$ which is calculated after ρ_3 reduces to the minimum value, but also by the factor [11]

$$S_{yM} = N^{-2} \left| \sum_{j}^{N} \exp[iM(2\pi/L_y^*) y_j^*] \right|^2 , \quad (8)$$

where M is the number of layers, and M is ≤ 5 due to the box side length L_y^*. The average $\langle\rho_j\rangle$ reflects the structural changes after equilibrium chains have broken. S_{yM} reflects the formation of layers, and $S_{yM} \geq 0.5$ signals perfect layers. Rheological properties are monitored by the relative viscosity η_r, which is derived from the stress $\langle\tau_{xz}\rangle$ of the particle interaction averaged over a simulation run,

$$\eta_r = -\langle\tau_{xz}\rangle/(\eta\dot{\gamma}) . \quad (9)$$

To study directly the relation between the variation of particle interactions and different structures of the suspension, we ignore the hydrodynamic contribution in Eq. (9).

III. RESULTS AND DISCUSSION

Based on an examination of the structures of suspensions by Eqs. (7) and (8) and snapshots at different state points (λ,Pe), the structural phase diagram for our system is constructed in Fig. 2. One can see from the figure that there exist three distinct single phases: liquid (L), shear string (S) and crystalline (C). In the liquid phase, when Pe=0, the particles are randomly distributed, and order parameters of the suspension have $\rho_j < 0.1$; while when Pe>0, although in shear flow short strings of particles can be formed down the compression axis, the distribution of these strings is still random, and the order parameters are $\langle\rho_1\rangle < 0.1$, $\langle\rho_2\rangle < 0.1$, and $\langle\rho_3\rangle < 0.3$. In the shear-string phase, the particles are positioned in strings which orient along the x direction and pack side by side into a distorted hexagonal lattice on the y-z plane. Within each string, there are only three to five irregularly spaced particles. The order parameters are $\langle\rho_1\rangle < 0.1$, $0.1 < \langle\rho_2\rangle < 0.23$, and $0.1 < \langle\rho_3\rangle < 0.3$. The factor S_{y5} decreases with time, and $S_{y5} \gg S_{yM}$ ($M = 2$, 3, and 4), and finally $S_{y5} < 0.5$. In the crystalline phase, when Pe=0, the particles either form a one-dimensional ordering gel-like structure

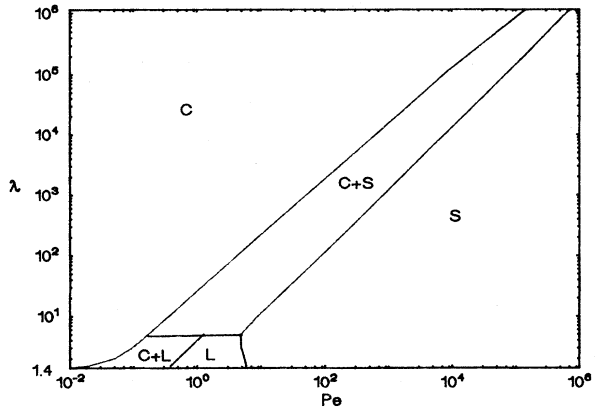

FIG. 2. The phase diagram: L, liquid phase; S, shear-string phase; C, crystalline phase; $C+S$ and $C+L$, coexistence phases.

with vertical simple chains aligned along the z direction or condense into a three-dimensional ordering bct lattice structure. The order parameters are $\rho_1>0.1$, $\rho_2>0.23$, and $\rho_3>0.5$. When Pe>0, the particles become a two-dimensional ordering layerlike structure, which lies in the x-z plane and has a well-defined layer spacing in the x-y plane. The order parameters are $\langle\rho_1\rangle>0.1$, $\langle\rho_2\rangle>0.23$, and $\langle\rho_3\rangle>0.5$. When the applied strain is less than 1, chains of particles within each layer stretch in the shear flow and are packed so that the alternate chains in the x direction are offset by half of an interparticle spacing to form a distorted close-packed-hexagonal lattice in the x-z plane. When the applied strain is greater than 1, the layers aggregate into thicker layers. For the layerlike structure, S_{y5} first decreases and then increases with time, but S_{yM} ($M=2$, 3, and 4) gradually increases and even becomes greater than S_{y5}, indicative of an aggregation of layers. Finally, the factor of the formed layer is higher than 0.5. In between these single phases there are the two two-phase coexistence zones, $C+L$ and $C+S$. In the former, the particles form unstable layers, being perturbed by the Brownian and shear forces but reformed by the dipolar force; the factor S_{yM} lies between 0.2 and 0.3. In the $C+S$ zone the particles aggregate in soft layers, being pulled apart by the shear force but reformed by the dipolar force; the factor S_{y5} first decreases with time. When the top electrode translates over $5L_x$, S_{y5} decreases to its minimum value, then begins to increase. But the other factors always increase with time, sometimes even higher than S_{y5}. The maximum of the final time factor is between 0.1 and 0.5. The order parameters for the suspension in these two-phase coexistence zones are $\langle\rho_1\rangle<0.1$, $\langle\rho_2\rangle>0.23$, and $0.1<\langle\rho_3\rangle<0.5$ for $C+L$, and $\langle\rho_1\rangle<0.1$, $0.1<\langle\rho_2\rangle<0.30$, and $0.3<\langle\rho_3\rangle<0.5$, or $\langle\rho_1\rangle<0.1$, $\langle\rho_2\rangle<0.1$, and $0.1<\langle\rho_3\rangle<0.3$ for $C+S$. Having defined the interparticle structures observed, we now examine the boundaries between the phases and the conditions which lead to these different structures.

A. Equilibrium structure

We studied the time evolution of a 3D structure in suspension in the static state (Pe=0). The simulation was performed for different values of λ from the same initial configuration. Figure 3 shows final time configurations of

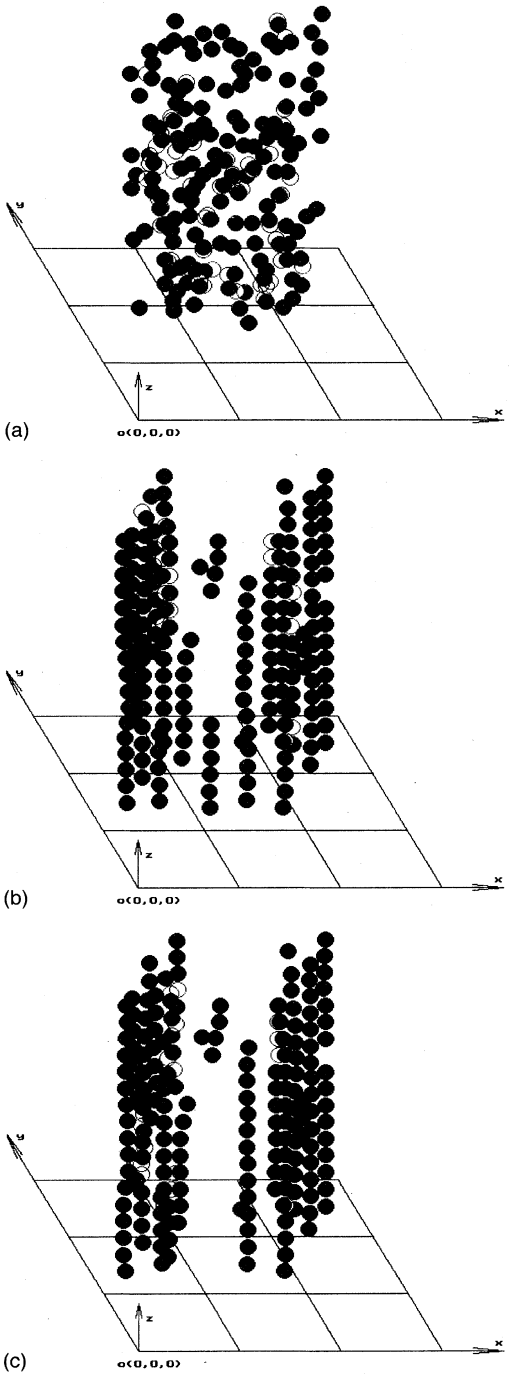

FIG. 3. Final configurations of suspensions: (a) λ=1, (b) λ=1 135 000, and (c) λ=113.5.

structures developed at three typical values of λ. Figure 4 shows the development of ρ_j with time in the above systems. It is clear that when λ is small (i.e., λ=1), the Brownian force is comparable to or even greater than the dipolar force. The suspension has too many vibrations, preventing the formation of a stable structure, so that the suspension is in the liquid phase regime. In this case, as shown in Figs. 3(a) and 4(a), particles are randomly distributed, and the order parameters remain less than 0.1. However, when λ is very

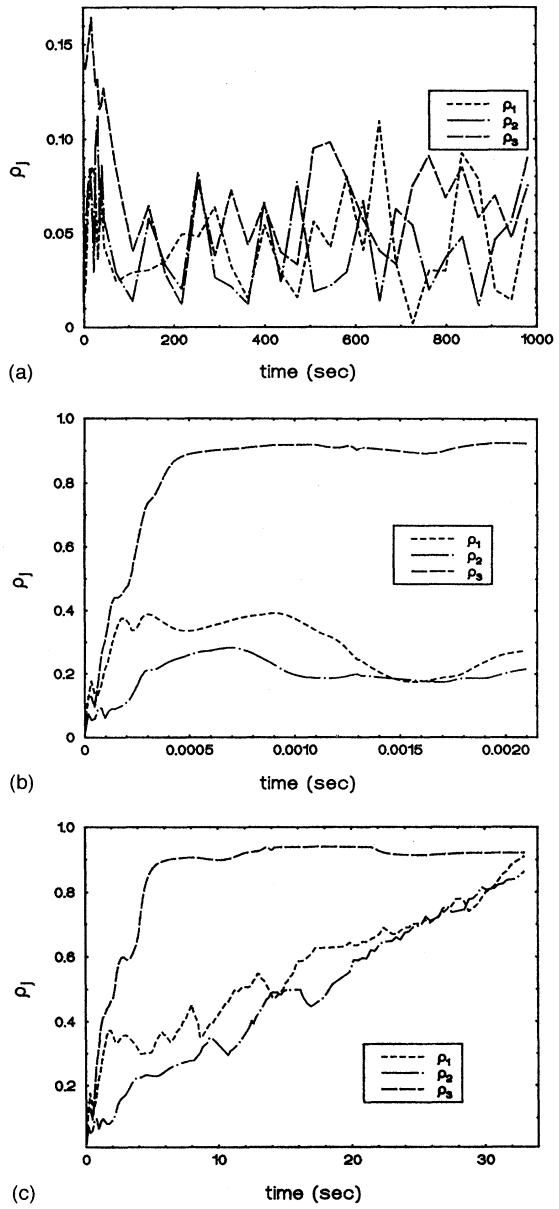

FIG. 4. Relationship of ρ_j with time for suspensions: (a) $\lambda=1$, (b) $\lambda=1\ 135\ 000$, and (c) $\lambda=113.5$.

large (i.e., $\lambda=1\ 135\ 000$), compared with the dipolar force the Brownian force is small enough to be neglected. The suspension becomes trapped into a complicated gel-like structure shown in Fig. 3(b), which has a rapid perfect ordering in the z direction and a weak lateral ordering in the x-y plane. As shown in Fig. 4(b), the order parameter ρ_3 achieves the maximum value 0.9 only after 1.21 ms, while ρ_2 and ρ_1 remain less than 0.4. When λ is moderate (i.e., $\lambda=113.5$), although the dipolar force dominates, the Brownian force cannot be ignored. The suspension condenses into thick columns which possess the bct lattice structure shown in Fig. 3(c). In this case, as shown in Fig. 4(c), the order parameter ρ_3 rapidly reaches the maximum value 0.94, while ρ_1 and ρ_2 increase slowly up to the maximum value 0.9. This means that, following rapid chain formation, the chains aggregate

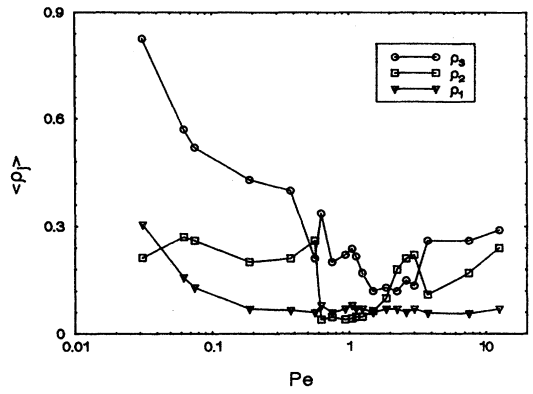

FIG. 5. Variation of $\langle\rho_j\rangle$ with Pe for the $\lambda=3$ suspension.

into the bct lattice structure. According to the simulation results in the static state case, the transition from disorder into a one-dimensional ordering chainlike structure occurs when $\lambda=1.4$, as shown in Fig. 2. Tao calculated the transition from the liquid state to the chainlike structure to be second order [12], so there is no two-phase zone between L and C for a fixed particle volume content ER suspension at Pe=0. For alumina particles of $\sigma=2$ μm in silicon oil at $T=300$ K, the critical electric field for the phase transition is 261.9 V/cm.

B. Nonequilibrium structure

To determine the phases in Fig. 2, we examine the structural changes of suspensions at different points (λ,Pe). Figures 5 and 6 show the variation of $\langle\rho_j\rangle$ and S_{yM} with Pe for different λ suspensions, respectively. Obviously for the $\lambda>5$ suspensions, the structures are dependent mainly on the dipolar and/or shear forces. Figures 7 and 8 show snapshots of the shear effect on the equilibrium configurations. When Pe $<\lambda/8$, the dipolar force is dominant, and suspensions aggregate into the stiff layerlike structure shown in Fig. 7. This structure allows homogeneous flow between layers because layers can slide readily in the flow direction. However, when Pe$>\lambda$, the shear force is dominant, and the suspensions flow into the shear-string structure shown in Fig. 8. This structure gives rise to the free slippage of strings. Between the above two values of Pe, the shear force is comparable to the dipolar force. Suspensions form an unstable layerlike structure, and

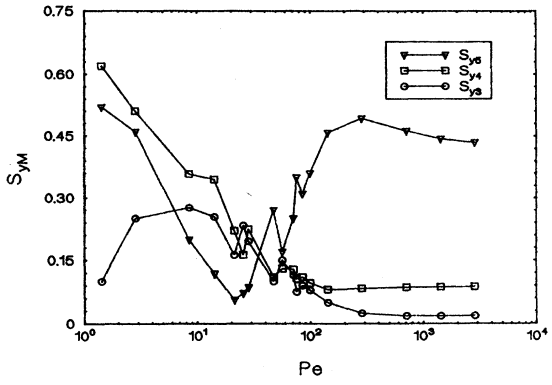

FIG. 6. Variation of S_{yM} with Pe for the $\lambda=113.5$ suspension.

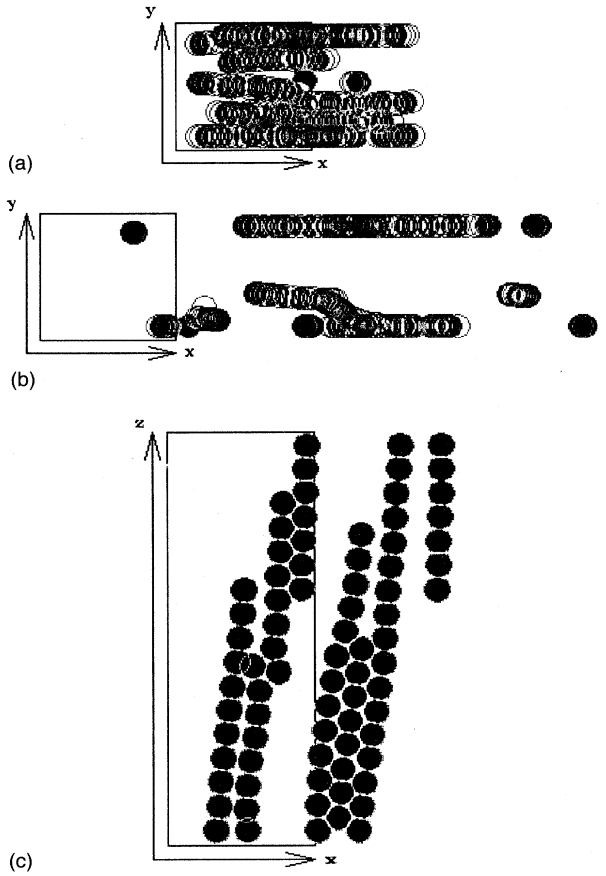

FIG. 7. Snapshot projections of the layerlike structure from Fig. 3(c) at Pe=1.42: (a) on the x-y plane at shear strain 0.4, (b) on the x-y plane at shear strain 1.0, and (c) one layer at shear strain 0.4.

the $C+S$ coexistence phase zone is located there. In simulation, we found that the curves of the boundaries between the C and $C+S$ phases and between the $C+S$ and S phases depend on the value of λ. With decreasing λ, the slope of the former curve increases, but the slope of the latter decreases.

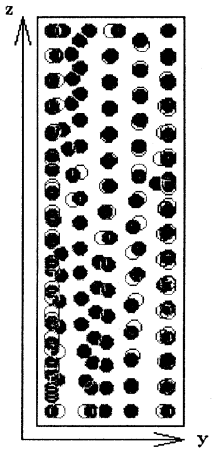

FIG. 8. Projection of the shear-string structure after shearing the equilibrium structure of $\lambda=11\,350$ at Pe=14 187 on the y-z plane.

This phenomenon is reasonable, because the layerlike structure is caused by the interaction of the strong dipolar force and the weak shear force, while the shear-string structure is caused by the interplay of the shear force and the repulsive force. The repulsive force is dependent on λ. With decreasing λ, the dipolar and repulsive forces decrease, but the random Brownian force increases. To overcome the Brownian effect and produce the layerlike structure, the maximum shear force needed at low λ should be smaller than the value calculated by the ratio of Pe/λ at high λ. But to overcome the Brownian effect and produce the shear-string structure, the minimum shear force needed at low λ should be greater than that value calculated by the ratio of Pe/λ at high λ. Hence, with decreasing λ, the slope of the C to $C+S$ boundary curve increases, while the slope of the $C+S$ to S boundary curve decreases. Obviously, such two boundary curves form a region like the two-phase zone in the phase transition of isomorphous systems. For $\lambda<1.4$ suspensions, the structures depend on the Brownian and/or shear forces. The continuous perturbation from the Brownian force makes suspensions in the liquid phase state. Even at high Pe, no shear string exists, due to the weak repulsive force. While for the suspensions of $1.4\leqslant\lambda\leqslant5$, the structures depend on the dipolar and/or the Brownian and/or the shear forces. When Pe$<\lambda/20$, suspensions are mainly controlled by the dipolar force. The vibration from the Brownian and/or shear interactions is not strong enough to break down the layerlike structure. However, when $\lambda/20<$Pe$<\lambda/4$, although layers of particles can be formed, they are unstable because the dipolar force is little stronger than the Brownian and shear forces. In this case, the crystalline phase and liquid phase coexist. Similarly, the slope of the C to $C+L$ boundary curve increases with decreasing λ. When $\lambda/4<$Pe$<\lambda$, the Brownian and shear forces become comparable to and/or greater than the dipolar force. No layerlike structure can be formed due to the perturbation from the Brownian and shear forces. Suspensions are in the liquid phase state. When Pe$>\lambda$, the shear force is much greater than the dipolar and Brownian forces, so the suspensions have a shear-string structure, and the slope of the boundary curve of L and S decreases with decreasing λ.

C. Rheological properties

Rheological properties are associated with the different structures adopted by the suspension under flow. Figure 9 shows the variation of the relative viscosity with increasing Pe for the different λ suspensions. We can see that for the shear-string phase, the suspension is in a shear thinning process: with the increase of Pe the viscosity drops and has a weak dependence on λ. The relationship is $\eta_r\propto\lambda^{\alpha}/\mathrm{Pe}^{\beta}$, where $0.96>\beta>0.25$ and $\beta>\alpha>0$. For the liquid phase, the viscosity is only dependent on Pe and $\eta_r\propto\mathrm{Pe}^{-\beta}$, $0.2<\beta$. With increasing Pe, the viscosity drops rapidly down close to zero. However, for the layerlike crystalline phase, the viscosity decreases with increasing Pe for a fixed λ, but increases with increasing λ for a fixed Pe. We have the relationship $\eta_r\propto(\lambda/\mathrm{Pe})^{0.6-0.96}$. The value of the index varies with λ: from 0.77 at $\lambda=2$ to 0.96 at $\lambda=11\,350$. For the case of an equal ratio value λ/Pe, the relative viscosity of a shearing bct equilibrium structure is higher than that of a shearing simple

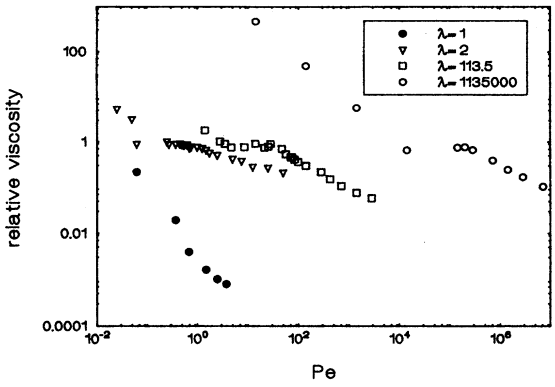

FIG. 9. Relative viscosity (η_r) against Pe for different λ suspensions.

chain equilibrium structure. Since the shear stress is mainly transmitted through chains and/or strands of particles, the flow of the layerlike phase is associated with the fluctuation of viscosity. Figure 10 shows a sequence of viscosity data against time for a layerlike system of $\lambda=113.5$ and $\mathrm{Pe}=1.42$. Figure 11 gives snapshots of a single layer corresponding to the times indicated by crosses in Fig. 10. We can see that the regular oscillations of viscosity are correlated with the strain-reform process observed in the snapshots. The viscosity maximum corresponds to maximum strain of chains straining in the flow direction and about to be broken, while viscosity approximates to zero when chains reform to nearly vertical chains after breaking. The transitions from the C to $C+S$ coexistence phase and from the C to $C+L$ coexistence phase appear in Fig. 9 as discontinuous increases of η_r. In the $C+S$ and $C+L$ phases, the viscosity oscillates weakly with increasing Pe. In our simulation we found that in the $C+S$ zone the viscosity reaches maximum and minimum values for a shear strain of 0.4 and 1.15, respectively, and approaches zero when a shear strain exceeds $\frac{5}{3}$. The dash-dot curve in Fig. 10 shows this sequence of viscosity for a $C+S$ phase at $\lambda=113.5$ at $\mathrm{Pe}=25.5$.

D. Interpretation of the structures and rheological properties

In the static state, for the $\lambda>1.4$ suspension, the structure is determined by minimizing the total electrostatic free energy. Since the dipolar free energy has its minimum when two dipoles join together and align in the field direction, the particles in the suspension first form chains between the two electrode plates upon the application of the electric field. Then the chains aggregate via one-dimensional Peierls-Landau dipole density fluctuation. For the high λ (i.e., $\lambda=1\ 135\ 000$) suspension, the initial process is much faster than the time in which the system relaxes into the columnar structure, so the chains aggregate into a distorted kinetically arrested gel-like structure. For the suspension with moderate λ (i.e., $\lambda=113.5$), the initial process slows down. The chains undergo a two-dimensional phase transition in the plane perpendicular to the electric field, and eventually evolve into the energetically favorable bct lattice. For the $\lambda<1.4$ suspension, the dominant Brownian effect leads to a random distribution of particles.

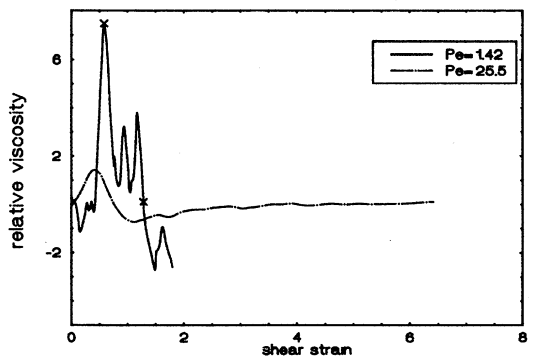

FIG. 10. Time sequence of the relative viscosity (η_r) for the $\lambda=113.5$ suspension at $\mathrm{Pe}=1.42$ and $\mathrm{Pe}=25.5$.

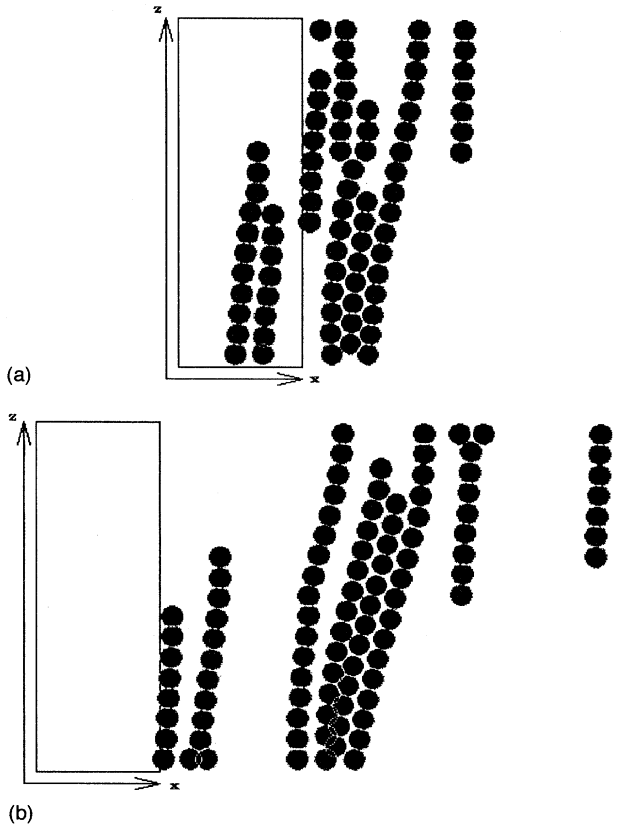

FIG. 11. Corresponding projections of the particles in a single layer taken at the time denoted by the crosses in Fig. 10.

In the dynamic state, the observed ordering is governed by the packing geometry of the particles, which allows flow in response to the applied strain. The interpretations of the suspension structures and resulting rheological properties are given below.

Layerlike structure (C). In this case, the interparticle dipolar force dominates over the shear and Brownian forces. (1) For the bct equilibrium structure under a shear, the layer spacings in Fig. 7(a) suggest that the bct close-packed planes (110) are slipping layers which lie in the x-z plane, and the bct $[1\bar{1}0]$ direction is in the flowing direction. In the simulation, the order parameters of the bct equilibrium structure is

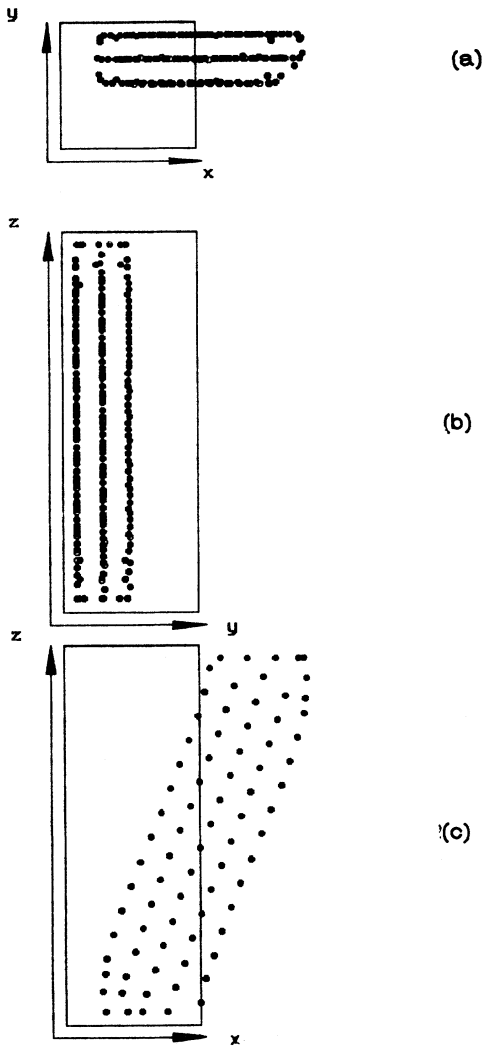

FIG. 12. Projections of the layerlike structure obtained by shearing the ideal bct equilibrium structure described (a) on the x-y plane, (b) on the y-z plane, and (c) on the x-z plane. Only the particle centers are shown.

less than 1. To verify whether the slipping layers and their slipping direction are indeed in the bct (110) plane and $[1\bar{1}0]$ direction, we assume an ideal bct structure with $\rho_j=1$ under shear. Figure 12 shows the projections of the resulting 3D layerlike structure on the three coordinate planes. We can see that this layerlike structure is the same as the layerlike structure shown in Fig. 7. In the x-y plane, layers stretch in the x direction and aggregate along the y direction, with a definite layer separation $\sqrt{3}/2\sigma$. In the y-z plane, each layer projects into a vertical chain along the z direction. In the x-z plane, particles within a layer form a close-packed-hexagonal structure. Obviously, to form such a layerlike structure, the bct (110) plane must be the slipping layer in the x-z plane, and the bct $[1\bar{1}0]$ direction must be the flowing direction in the x direction. In the presence of shear, since there exist long-range dipolar and short-range repulsive interactions between particles, the registered stacking of the layers [bct (110) planes] is defined to be *ABAB*—shown in Fig. 13. In such a

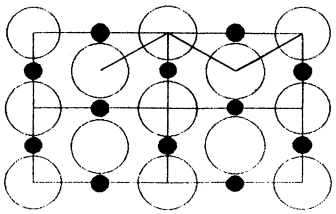

FIG. 13. The registered stacking of layers and the zigzag path adopted by a particle in the flow field. The particle positions in layer A are marked by ●, and these in layer B by ○.

geometric packing, the layers can slip readily, while, within each layer, the particles must adopt a zigzag path to slide over neighboring particles, as shown in Fig. 13. This is because the flow velocities of particles in a layer depend on their positions in the z direction. The zigzag motion is apparent in our simulation. The solid curve in Fig. 14 shows the sequence of z_j of one particle in the layer of Fig. 7(c). It seems that the zigzag motion is related to the fluctuations of the layerlike structure and its viscosity. For the layerlike structure at constant shear rate Pe, as λ increases, the interaction between particles increases, and so does the resulting viscosity; while for fixed λ, as Pe increases, the particle interaction decreases and the resulting viscosity drops. Due to the dominance of the interparticle dipolar force, particles in different layers can aggregate during the shearing process, which leads to the formation of thick layers. (2) For the simple vertical chain equilibrium structure under a shear, there also exist an interparticle long-range dipolar force and a short-range repulsive force. The particles condense into layers, and the layers stacking into a 3D structure are defined to be *ABAB*. Examination of snapshots of the suspension at $\lambda=1\ 135\ 000$ and $\mathrm{Pe}=14\ 187.5$ shows that the close-packed layers lie in the x-z plane, and the non-close-packed direction is parallel to the flowing direction. Similarly, in the presence of shear, the layer can slip readily, while within each layer particles move along a zigzag path to slide over neighboring particles. The resulting structure and rheological property are the same as that in case (1).

Coexistence of the layerlike and shear-string structures ($C+S$). In this case, the dipolar force is comparable to the

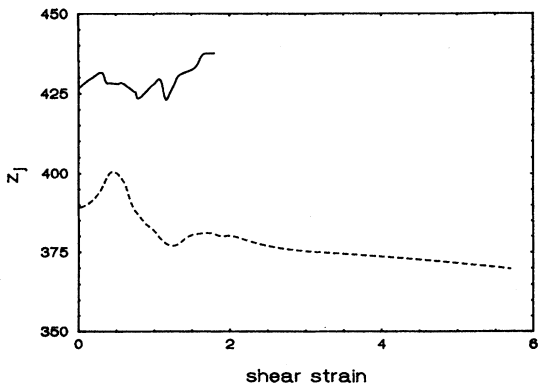

FIG. 14. Sequence of z_j of one particle. The solid curve indicates the particle in the layer; the dashed curve indicates the particle in the $C+S$ phase.

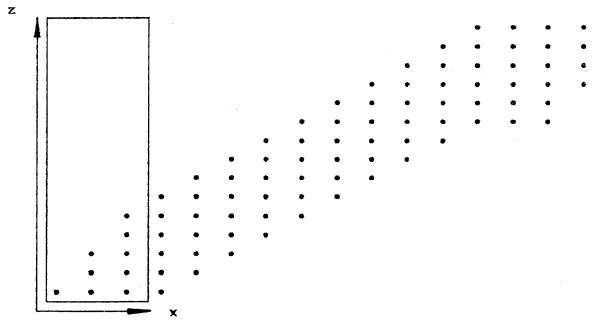

FIG. 15. $C+S$ structure in the x-z plane when the top electrode translates over $5L_x$. Only the particle centers are shown.

shear force, and the interparticle force becomes weaker than that in the layerlike structure. For the bct equilibrium structures under a shear, there is weak registration between the neighboring particles. The particles condense into unstable, locally distorted, close-packed-hexagonal layers which stack upon one another with an irregular layer separation. Similar to the layerlike structure, the unstable close-packed layers are in the x-z plane, and the nonclose-packed direction within one layer is parallel to the x direction. In a shear flow, layers can slide freely, but particles within one layer first take a zigzag path and then a straight line to move over each other. This phenomenon is apparent in our simulation. The dashed curve in Fig. 14 shows z_j of a particle in the $C+S$ structure with time. We can see that the particle adopts a zigzag motion prior to being sheared over $5L_x$ and takes a straight path after that. In the $C+S$ phase, the dipolar force is comparable to the shear force. If we do not take account of the repulsive particle interaction and the zigzag motion of particles within each layer, according to the simulation cell geometry, when the top electrode translates over $5L_x$ along the x direction, the distance of the nearest-neighboring particles should attain its minimum value $\sigma/2$, the strained chains of particles should return to vertical short chains along the z direction, and stress and viscosity should drop down to their minimum values. In fact, however, the repulsive force always pulls the particles apart, and the particles move along a zigzag path to minimize collision. Therefore, when the top electrode translates over $5L_x$, the distance of the nearest-neighboring particles becomes σ, the strained chains grow as the vertical short chains, and the stress and viscosity decrease to zero. Figure 15 shows such a $S+C$ structure in the x-z plane by shearing an ideal bct equilibrium structure with $\rho_j=1$ when the top electrode translates $5L_x$. In this case, the distance of neighboring chains in the x direction is $\sqrt{3}\sigma$, while the distance of neighboring chains in the y direction is $\sqrt{3}/2\sigma$. The short chains begin to aggregate

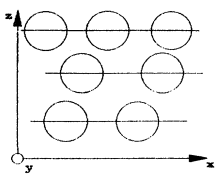

FIG. 16. Depiction of the shear-string structure in the x-z plane.

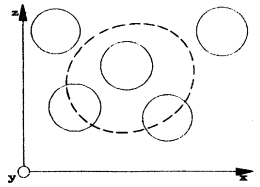

FIG. 17. Depiction of the liquid phase structure under a shear in the x-z plane.

in the y direction, and the factor S_{y5} decreases to its minimum value. But because of weak interparticle interaction and shear force this aggregation is rather weak; some short vertical chains may aggregate and others not, leading to irregular layer-separation spacings. In this case, other factors may increase above S_{y5}, but the final time factor maximum should be less than 0.5. The discontinuous increase in viscosity from the C to $C+S$ phases results from the breaking of the structure symmetry. Because the layers are unstable, the viscosity oscillates instead of decreasing with increase of Pe. All results are consistent with the case of the shearing simple chain equilibrium structure.

Shear-string structure (S). In this case, the shear force dominates over the dipolar and/or Brownian forces. The interparticle interaction will be much weaker than that in the $C+S$ structure. There is less registration between the neighboring particles. For the bct and/or simple chain equilibrium structures under a shear, the close-packed layers and definite registered stacking have broken down. The randomly spaced short chains stretch along the shear flow direction, leaving strings of particles parallel to the x direction, as shown in Fig. 16. In such a structure, the strings form distorted hexagonal arrays in the y-z plane shown in Fig. 8, and within each string there are several irregularly spaced particles due to reduced interparticle registration. The strings and particles can slip straight along the x direction without collisions, so the resulting viscosity has weak dependence on λ and decreases with increase of Pe.

Liquid structure (L). In this case, the Brownian force and/or the shear force are comparable to or even dominant over the dipolar force. There is rather low interparticle interaction, and no registration between the neighboring particles. For the simple chain and liquid equilibrium structures under a shear, the particles assume a distorted isotropic distribution as shown in Fig. 17. In such a structure, since particles lack interaction, the viscosity of the suspension rapidly drops to approximately zero as Pe increases.

Coexistence of the layerlike and liquid structures ($C+L$). In this case, the dipolar force is not much larger than the Brownian and shear forces. The interparticle interaction becomes weaker than that in the layerlike structure. For the simple chain equilibrium structures under a shear, the unstable local distorted closed-packed-hexagonal layers align in the x-z plane, but orient to produce the maximum resistance to continuous slipping of layers and of particles within a layer. Therefore from the C to $C+L$ phase, the viscosity does not decrease, the layers tumble in the shear flow, and the resulting viscosity oscillates with increasing Pe.

IV. CONCLUSION

The structural phase diagram of ER fluids has been con-

structed. There exist three single phases: layerlike or chainlike crystalline phase (C), shear-string phase (S), and liquid phase (L). Between these single phases there are two-phase coexistence zones of $C+S$ and $C+L$. In different phase zones, the viscosities of the suspensions have different relationships with Pe and λ. Interpretations of the observed structures and the resulting rheological properties have been discussed.

[1] Thomas C. Halsey and James E. Martin, Sci. Am. **81**, 42 (1993).
[2] W. M. Winslow, J. Appl. Phys. **20**, 1137 (1949).
[3] D. L. Klass and T. W. Martinek, J. Appl. Phys. **38**, 75 (1967).
[4] D. Brooks, Phys. World **2**, 35 (1989).
[5] K. C. Hass, Phys. Rev. E **47**, 3362 (1993).
[6] R. Tao and Qi Jiang, Phys. Rev. Lett. **73**, 205 (1994).
[7] R. T. Bonnecaze and J. F. Brady, J. Chem. Phys. **96**, 2183 (1992).
[8] D. M. Heyes, J. Non-Newtonian Fluid Mech. **27**, 47 (1988).
[9] M. Whittle, J. Non-Newtonian Fluid Mech. **37**, 233 (1990).
[10] D. J. Klingenberg, F. van Swol, and C. F. Zukoski, J. Chem. Phys. **91**, 85 (1989); **94**, 6160 (1991).
[11] J. R. Melrose, Mol. Phys. **76**, 635 (1992).
[12] R. Tao, Phys. Rev. E **47**, 423 (1993).